Gridless Super-Resolution Direction Finding for Strictly Non-Circular Sources Based on Atomic Norm Minimization

Jens Steinwandt [1], *Florian Roemer* [2], *Christian Steffens* [3], *Martin Haardt* [1], *and Marius Pesavento* [3]

[1] Communications Research Laboratory, Ilmenau University of Technology, P.O. Box 100565, 98684 Ilmenau, Germany
[2] Digital Broadcasting Laboratory, Ilmenau University of Technology, P.O. Box 100565, 98684 Ilmenau, Germany
[3] Communication Systems Group, TU Darmstadt, Merckstraße 25, 64283 Darmstadt, Germany
Emails: {jens.steinwandt, florian.roemer, martin.haardt}@tu-ilmenau.de, {steffens, pesavento}@nt.tu-darmstadt.de

***Abstract*—The recently developed super-resolution framework by Candés enables direction-of-arrival (DOA) estimation from a sparse spatial power spectrum in the continuous domain with infinite precision in the noise-free case. By means of atomic norm minimization (ANM), the discretization of the spatial domain is no longer required, which overcomes the basis mismatch problem in conventional sparse signal recovery (SSR)-based DOA estimation. In this paper, we incorporate additional signal structure, i.e., the strict second-order non-circularity (NC) of the signals, into the ANM framework for the noisy multiple measurement vector (MMV) model. Due to the NC preprocessing step, the NC ANM problem provides a two-level Hermitian Toeplitz structured solution matrix, which possesses a two-dimensional Vandermonde decomposition such that desired the spatial frequencies can be uniquely extracted via NC Standard/Unitary ESPRIT in closed-form. The presented NC ANM procedure efficiently exploits the NC signal structure, resulting in both a reduced estimation error and an increased source identifiability compared to the conventional ANM approach. Simulation results demonstrate the superior performance of the proposed method.**

***Index Terms*—Super-resolution, atomic norm minimization, gridless compressive sensing, non-circular sources, DOA estimation.**

I. Introduction

Direction-of-arrival (DOA) estimation of impinging signals is of high importance in many applications involving array signal processing [1], e.g., radar, sonar, channel sounding, wireless communications. A particularly challenging scenario for DOA estimation is the resolution of two or more closely-spaced sources with high precision from very few data snapshots. It has recently been shown that sparse signal recovery (SSR)-based DOA estimation algorithms [2], [3], which exploit the compressed sensing (CS) paradigm [4], [5], can provide an improved estimation accuracy over the conventional high-resolution parameter estimation algorithms [1] in such challenging scenarios. However, these SSR-based algorithms rely on the discretization of the spatial domain to form an overcomplete basis, which results in a basis mismatch problem if the DOAs lie off the discretized grid.

The super-resolution framework recently developed in [6] and [7] provides a new perspective of SSR-based parameter estimation by proposing a gridless sparse recovery procedure by means of atomic norm minimization (ANM) for a single measurement vector (SMV). Thereby, the sparse spatial line spectrum can be recovered in the continuous parameter domain with infinite precision in the noiseless case [6], [7]. Specifically, solving the ANM-equivalent semidefinite programming (SDP) problem provides a Hermitian Toeplitz structured solution matrix, which admits a unique Vandermonde decomposition such that the set of DOAs can be uniquely recovered from the solution via conventional parameter estimation algorithms [1]. An extension to the multiple measurement vector (MMV) case is given in [8] and a multi-dimensional extension of the ANM framework for multi-dimensional parameter estimation is provided in [9], [10]. In the latter, it is shown that the multi-dimensional ANM problem produces a multi-level Hermitian Toeplitz matrix, which still admits a unique Vandermonde decomposition involving a Kronecker structure. Therefore, the multi-dimensional spatial frequencies can be uniquely recovered from the obtained multi-level Hermitian Toeplitz matrix. A major drawback of the ANM approach is that it suffers from the so-called resolution limit, i.e., the spatial frequencies can only be recovered if they are sufficiently separated [6], [7].

Previous work has shown that the performance of the conventional DOA estimation algorithms [1] can be further improved if inherent structure of the received signals, i.e., their strictly second-order (SO) non-circularity (NC) [11], is exploited. Such NC signals result from real-valued modulation schemes such as BPSK, PAM, ASK, Offset-QPSK (after a de-rotation), etc. Numerous subspace-based parameter estimation algorithms [12]-[15] that exploit this structure achieve an improved estimation accuracy and double the number of identifiable sources. In [16] and [17], two CS-based DOA estimation algorithms for the SSR of NC signals have recently been proposed. The former results in a 2-D recovery problem as it requires the additional sampling of the rotation phase domain along with the spatial domain in order to account for the arbitrary rotation phases of the NC signals. In contrast, the algorithm in [17] reduces the 2-D problem in [16] to a 1-D recovery problem by means of nuclear norm minimization. However, both NC methods rely on the discretization of the spatial domain, making a gridless SSR version for NC signals highly desirable.

In this paper, we develop a gridless super-resolution framework based on ANM for strictly non-circular signals. Specifically, we adopt the MMV model and show that after applying the NC preprocessing step, the resulting NC ANM SDP problem provides a solution matrix with a two-level Hermitian Toeplitz structure. Applying the multi-dimensional generalization of the Vandermonde decomposition in [10], the desired spatial frequencies are uniquely extracted from the two-level Hermitian Toeplitz matrix via NC Standard/Unitary ESPRIT [15] in closed-form. Simulation results show that in the case of NC signals, the proposed NC ANM method attains a superior estimation performance over the original ANM approach for a small sample size and a low signal-to-noise ratio (SNR) and can resolve more sources than sensors are present. Moreover, due to the decoupling effect of two NC sources with maximum phase separation, the proposed NC ANM algorithm does not suffer from the resolution limit in this case.

This work was supported by the EXPRESS project within the DFG priority program CoSIP (DFG-SPP 1798) and the Carl-Zeiss Foundation under the scholarship project EMBiCoS.

II. System Model

Assume that a uniform linear array (ULA)[1] consisting of M isotropic elements receives narrowband signals from d far-field sources. The N subsequent observations can be modeled as

$$\boldsymbol{X} = \boldsymbol{A}(\boldsymbol{\mu})\boldsymbol{S} + \boldsymbol{N} \in \mathbb{C}^{M\times N}, \tag{1}$$

where $\boldsymbol{A}(\boldsymbol{\mu}) = [\boldsymbol{a}(\mu_1), \dots, \boldsymbol{a}(\mu_d)] \in \mathbb{C}^{M\times d}$ is the array steering matrix, which contains the array steering vectors $\boldsymbol{a}(\mu_i)$, $i = 1, \dots, d$, for the spatial frequencies $\boldsymbol{\mu} = [\mu_1, \dots, \mu_d]^{\mathrm{T}}$. The matrix $\boldsymbol{S} \in \mathbb{C}^{d\times N}$ represents the source symbol matrix, and $\boldsymbol{N} \in \mathbb{C}^{M\times N}$ consists of the additive sensor noise samples with variance σ_{n}^2.

In the case of strictly SO non-circular sources, the received complex symbol amplitudes of each source lie on a rotated line in the complex plane. Therefore, $\boldsymbol{S}$ can be written as $\boldsymbol{S} = \boldsymbol{\Psi}(\boldsymbol{\varphi})\boldsymbol{S}_0$, where $\boldsymbol{S}_0 \in \mathbb{R}^{d\times N}$ is a real-valued symbol matrix and $\boldsymbol{\Psi}(\boldsymbol{\varphi}) = \mathrm{diag}\{\mathrm{e}^{\mathrm{j}\varphi_i}\}_{i=1}^{d}$ contains the complex phase shifts corresponding to the phases $\boldsymbol{\varphi} = [\varphi_1, \dots, \varphi_d]^{\mathrm{T}}$ on its diagonal that are usually different for each received signal [15]. In order to take advantage of this property, we apply a preprocessing scheme to (1) and define the augmented measurement matrix $\boldsymbol{X}^{(\mathrm{nc})} \in \mathbb{C}^{2M\times N}$ as [14], [15]

$$\begin{aligned}\boldsymbol{X}^{(\mathrm{nc})} &= \begin{bmatrix}\boldsymbol{X}\\ \boldsymbol{\Pi}_M\boldsymbol{X}^*\end{bmatrix} = \begin{bmatrix}\boldsymbol{A}(\boldsymbol{\mu})\boldsymbol{\Psi}(\boldsymbol{\varphi})\\ \boldsymbol{\Pi}_M\boldsymbol{A}^*(\boldsymbol{\mu})\boldsymbol{\Psi}^*(\boldsymbol{\varphi})\end{bmatrix}\boldsymbol{S}_0 + \begin{bmatrix}\boldsymbol{N}\\ \boldsymbol{\Pi}_M\boldsymbol{N}^*\end{bmatrix}\\ &= \boldsymbol{A}^{(\mathrm{nc})}(\boldsymbol{\mu},\boldsymbol{\varphi})\boldsymbol{S}_0 + \boldsymbol{N}^{(\mathrm{nc})} = \boldsymbol{X}_0^{(\mathrm{nc})} + \boldsymbol{N}^{(\mathrm{nc})},\end{aligned} \tag{2}$$

where $\boldsymbol{X}_0^{(\mathrm{nc})}$ denotes the noise-free NC measurement matrix and $\boldsymbol{\Pi}_M$ is the $M \times M$ exchange matrix with ones on its anti-diagonal and zeros elsewhere. The extended dimensions of $\boldsymbol{A}^{(\mathrm{nc})}(\boldsymbol{\mu},\boldsymbol{\varphi}) \in \mathbb{C}^{2M\times d}$ can be interpreted as a virtual doubling of the sensor elements, which improves the estimation performance and doubles the number of detectable sources.

The $(2M \times 2M)$ spatial covariance matrix of (2) is given by

$$\boldsymbol{R}^{(\mathrm{nc})} = \frac{1}{N}\mathbb{E}\left\{\boldsymbol{X}^{(\mathrm{nc})}\boldsymbol{X}^{(\mathrm{nc})^{\mathrm{H}}}\right\} = \begin{bmatrix}\boldsymbol{R} & \boldsymbol{C}\boldsymbol{\Pi}_M\\ \boldsymbol{\Pi}_M\boldsymbol{C}^* & \boldsymbol{\Pi}_M\boldsymbol{R}^*\boldsymbol{\Pi}_M\end{bmatrix}, \tag{3}$$

where

$$\begin{aligned}\boldsymbol{R} &= \frac{1}{N}\mathbb{E}\{\boldsymbol{X}\boldsymbol{X}^{\mathrm{H}}\}\\ &= \boldsymbol{A}(\boldsymbol{\mu})\boldsymbol{\Psi}(\boldsymbol{\varphi})\boldsymbol{R}_{\boldsymbol{S}_0}\boldsymbol{\Psi}^*(\boldsymbol{\varphi})\boldsymbol{A}^{\mathrm{H}}(\boldsymbol{\mu}) + \sigma_{\mathrm{n}}^2\boldsymbol{I}_M \in \mathbb{C}^{M\times M},\end{aligned} \tag{4}$$

$$\begin{aligned}\boldsymbol{C} &= \frac{1}{N}\mathbb{E}\{\boldsymbol{X}\boldsymbol{X}^{\mathrm{T}}\}\\ &= \boldsymbol{A}(\boldsymbol{\mu})\boldsymbol{\Psi}(\boldsymbol{\varphi})\boldsymbol{R}_{\boldsymbol{S}_0}\boldsymbol{\Psi}(\boldsymbol{\varphi})\boldsymbol{A}^{\mathrm{T}}(\boldsymbol{\mu}) \in \mathbb{C}^{M\times M}\end{aligned} \tag{5}$$

represent the covariance matrix and the pseudo-covariance matrix, respectively, and $\boldsymbol{R}_{\boldsymbol{S}_0}$ is the real-valued signal covariance matrix $\boldsymbol{R}_{\boldsymbol{S}_0} = \frac{1}{N}\mathbb{E}\{\boldsymbol{S}_0\boldsymbol{S}_0^{\mathrm{T}}\} \in \mathbb{R}^{d\times d}$.

Recall that the assumption of the centro-symmetry of the array implies that $\boldsymbol{\Pi}_M\boldsymbol{A}^*(\boldsymbol{\mu}) = \boldsymbol{A}(\boldsymbol{\mu})\boldsymbol{\Delta}$ holds, where $\boldsymbol{\Delta} \in \mathbb{C}^{d\times d}$ is a unitary diagonal matrix that depends on the phase reference of the array. Applying this property to (2), the augmented array steering matrix simplifies to

$$\boldsymbol{A}^{(\mathrm{nc})}(\boldsymbol{\mu},\boldsymbol{\varphi}) = \begin{bmatrix}\boldsymbol{A}(\boldsymbol{\mu})\boldsymbol{\Psi}(\boldsymbol{\varphi})\\ \boldsymbol{A}(\boldsymbol{\mu})\boldsymbol{\Delta}\boldsymbol{\Psi}^*(\boldsymbol{\varphi})\end{bmatrix}. \tag{6}$$

If we additionally assume uncorrelated signals, such that $\boldsymbol{R}_{\boldsymbol{S}_0}$ is a diagonal matrix, the NC covariance matrix of (3) reduces to

$$\boldsymbol{R}^{(\mathrm{nc})} = \begin{bmatrix}\boldsymbol{R} & \boldsymbol{C}\\ \boldsymbol{C}^{\mathrm{H}} & \boldsymbol{R}\end{bmatrix}, \tag{7}$$

[1]The assumption of a ULA can also be relaxed to a centro-symmetric non-uniform linear array (NULA), which differs from a ULA only by some missing sensor elements while still being centro-symmetric.

where $\boldsymbol{R}$ from (4) simplifies to $\boldsymbol{R} = \boldsymbol{A}(\boldsymbol{\mu})\boldsymbol{R}_{\boldsymbol{S}_0}\boldsymbol{A}^{\mathrm{H}}(\boldsymbol{\mu}) + \sigma_{\mathrm{n}}^2\boldsymbol{I}_M$ and $\boldsymbol{C}$ from (5) simplifies to $\boldsymbol{C} = \boldsymbol{A}(\boldsymbol{\mu})\boldsymbol{\Psi}(\boldsymbol{\varphi})\boldsymbol{R}_{\boldsymbol{S}_0}\boldsymbol{\Psi}(\boldsymbol{\varphi})\boldsymbol{\Delta}^*\boldsymbol{A}^{\mathrm{H}}(\boldsymbol{\mu})$, respectively. Note that both $\boldsymbol{R}$ and $\boldsymbol{C}$ possess a Toeplitz structure. Thus, (7) exhibits a two-level Hermitian Toeplitz structure, also referred to as Hermitian Toeplitz-block-Toeplitz matrix [10], which is defined as

$$\boldsymbol{T} = \begin{bmatrix}\boldsymbol{T}_1 & \boldsymbol{T}_2\\ \boldsymbol{T}_2^{\mathrm{H}} & \boldsymbol{T}_1\end{bmatrix} \in \mathbb{C}^{2M\times 2M}, \tag{8}$$

where the blocks $\boldsymbol{T}_n \in \mathbb{C}^{M\times M}$, $n = 1, 2$, are Toeplitz as well.

III. NC Atomic Norm Minimization

In this section, we introduce the atomic norm minimization (ANM) concept for the gridless sparse reconstruction of signals with NC structure using the MMV model. In particular, we extend the original ANM framework [7] that does not consider signal structure and incorporate the prior knowledge of the statistical properties of NC signals in order to improve the reconstruction performance. Due to the unknown arbitrary rotation phase of the NC signals, the signal reconstruction problem naturally becomes a 2-D ANM problem, which involves sparse recovery in the spatial domain as well as in the rotation phase domain. Therefore, we apply [10] that considers ANM for higher dimensional estimation problems.

A. Proposed NC Atomic Norm Minimization Algorithm

In this section, we present the main steps of the proposed NC ANM approach for NC signals. For simplicity and without loss of generality, we assume that the phase reference of the array is located at the array centroid, i.e., $\boldsymbol{\Delta} = \boldsymbol{I}_d$, such that the array steering vector corresponding to the i-th spatial frequency is given by

$$\boldsymbol{a}(\mu_i) = \left[\mathrm{e}^{-\mathrm{j}\frac{M-1}{2}\mu_i} \quad \dots \quad \mathrm{e}^{\mathrm{j}\frac{M-1}{2}\mu_i}\right]^{\mathrm{T}} \in \mathbb{C}^{M\times 1}. \tag{9}$$

Then, the NC steering matrix $\boldsymbol{A}^{(\mathrm{nc})}(\boldsymbol{\mu},\boldsymbol{\varphi})$ in (2) can be compactly expressed as

$$\boldsymbol{A}^{(\mathrm{nc})}(\boldsymbol{\mu},\boldsymbol{\varphi}) = \boldsymbol{\Phi}(\boldsymbol{\varphi}) \diamond \boldsymbol{A}(\boldsymbol{\mu}), \tag{10}$$

where $\boldsymbol{\Phi}(\boldsymbol{\varphi}) = [\boldsymbol{\psi}_1, \dots, \boldsymbol{\psi}_d] \in \mathbb{C}^{2\times d}$ with $\boldsymbol{\psi}_i = [\mathrm{e}^{\mathrm{j}\varphi_i}, \mathrm{e}^{-\mathrm{j}\varphi_i}]^{\mathrm{T}} \in \mathbb{C}^{2\times 1}$, $\boldsymbol{A}(\boldsymbol{\mu})$ given in (1) contains the steering vectors according to (9), and $\diamond$ denotes the Khatri-Rao product (the column-wise Kronecker product).

Using (10), we can rewrite the noise-free NC measurement matrix from (2) as

$$\boldsymbol{X}_0^{(\mathrm{nc})} = \sum_{i=1}^{d}\boldsymbol{a}^{(\mathrm{nc})}(\mu_i,\varphi_i)\boldsymbol{s}_{0_i}^{\mathrm{T}} = \sum_{i=1}^{d}\left(\begin{bmatrix}\mathrm{e}^{\mathrm{j}\varphi_i}\\ \mathrm{e}^{-\mathrm{j}\varphi_i}\end{bmatrix} \otimes \boldsymbol{a}(\mu_i)\right)\boldsymbol{s}_{0_i}^{\mathrm{T}}, \tag{11}$$

where $\boldsymbol{a}^{(\mathrm{nc})}(\mu_i,\varphi_i)$ and $\boldsymbol{s}_{0_i}^{\mathrm{T}}$ represent the i-th column of $\boldsymbol{A}^{(\mathrm{nc})}(\boldsymbol{\mu},\boldsymbol{\varphi})$ in (10) and the i-th row of $\boldsymbol{S}_0$, respectively, and $\otimes$ symbolizes the Kronecker product. The Kronecker structure of $\boldsymbol{a}^{(\mathrm{nc})}(\mu_i,\varphi_i)$ reveals the separability of the spatial and the rotation phase parameters. Moreover, it is apparent that (11) is sparse in both dimensions as only a few respective components are present.

In consistence with the ANM framework, which exploits the sparsity in the continuous parameter space by means of the atomic norm metric, we define the atoms

$$\tilde{\boldsymbol{X}}_0^{(\mathrm{nc})}(\tilde{\mu},\tilde{\varphi},\tilde{\boldsymbol{s}}_0) = \boldsymbol{a}^{(\mathrm{nc})}(\tilde{\mu},\tilde{\varphi})\tilde{\boldsymbol{s}}_0^{\mathrm{T}}, \tag{12}$$

where $\tilde{\mu} \in [-\pi, \pi)$, $\tilde{\varphi} \in [0, 2\pi)$ and $\tilde{\boldsymbol{s}}_0 \in \mathbb{R}^{N\times 1}$ with $\|\tilde{\boldsymbol{s}}_0\|_2 = 1$. Subsequently, the continuous dictionary, also termed atomic set, is given by

$$\mathcal{A} = \left\{\tilde{\boldsymbol{X}}_0^{(\mathrm{nc})}(\tilde{\mu},\tilde{\varphi},\tilde{\boldsymbol{s}}_0) \mid \tilde{\mu} \in [-\pi,\pi),\ \tilde{\varphi} \in [0,2\pi),\ \|\tilde{\boldsymbol{s}}_0\|_2 = 1\right\}.$$

According to [8], the atomic ℓ_0-norm is defined as

$$\begin{aligned}&\left\|\boldsymbol{X}_0^{(\mathrm{nc})}\right\|_{\mathcal{A},0}\\&=\inf_{\substack{\{\tilde{\mu}_k,\\ \tilde{\varphi}_k,\tilde{\boldsymbol{s}}_{0_k}\}}}\left\{K\;\middle|\;\boldsymbol{X}_0^{(\mathrm{nc})}=\sum_{k=1}^{K}c_k\tilde{\boldsymbol{X}}_0^{(\mathrm{nc})}(\tilde{\mu}_k,\tilde{\varphi}_k,\tilde{\boldsymbol{s}}_{0_k}),\;c_k\geq 0\right\}\end{aligned}\tag{13}$$

and describes the smallest number of atoms to compose $\boldsymbol{X}_0^{(\mathrm{nc})}$. A natural objective to obtain $\boldsymbol{X}_0^{(\mathrm{nc})}$ is to minimize $\|\boldsymbol{X}_0^{(\mathrm{nc})}\|_{\mathcal{A},0}$, i.e., to find the atomic decomposition of $\boldsymbol{X}_0^{(\mathrm{nc})}$ with the minimal number of atoms while still being consistent with the noise-corrupted NC data matrix $\boldsymbol{X}^{(\mathrm{nc})}$. Following the lines of [7], the minimization of the atomic ℓ_0-norm in (13) can be equivalently characterized as the rank minimization problem

$$\begin{aligned}&\min_{\boldsymbol{W},\boldsymbol{T}}\quad \mathrm{rank}\{\boldsymbol{T}\}\\&\text{s. t.}\quad \begin{bmatrix}\boldsymbol{W} & \boldsymbol{X}_0^{(\mathrm{nc})\mathrm{H}}\\ \boldsymbol{X}_0^{(\mathrm{nc})} & \boldsymbol{T}\end{bmatrix}\succeq\boldsymbol{0},\;\left\|\boldsymbol{X}^{(\mathrm{nc})}-\boldsymbol{X}_0^{(\mathrm{nc})}\right\|_{\mathrm{F}}^2\leq\eta^{(\mathrm{nc})},\end{aligned}\tag{14}$$

where the solution matrix $\boldsymbol{T}$ is a two-level Hermitian Toeplitz matrix in accordance with (8) and $\eta^{(\mathrm{nc})}$ is the regularization parameter. As the rank minimization problem (14) is non-convex and NP-hard, we instead consider the convex ℓ_1-relaxation of the atomic ℓ_0-norm, also referred to as the atomic ℓ_1-norm, which is defined as

$$\begin{aligned}&\|\boldsymbol{X}_0^{(\mathrm{nc})}\|_{\mathcal{A}}\\&=\inf_{\substack{\{\tilde{\mu}_k,\\ \tilde{\varphi}_k,\tilde{\boldsymbol{s}}_{0_k}\}}}\left\{\sum_k c_k\;\middle|\;\boldsymbol{X}_0^{(\mathrm{nc})}=\sum_k c_k\tilde{\boldsymbol{X}}_0^{(\mathrm{nc})}(\tilde{\mu}_k,\tilde{\varphi}_k,\tilde{\boldsymbol{s}}_{0_k}),\;c_k\geq 0\right\}.\end{aligned}$$

Again following [7], the corresponding atomic ℓ_1-norm minimization problem admits the following SDP formulation

$$\begin{aligned}&\min_{\boldsymbol{W},\boldsymbol{T}}\quad \frac{1}{2}\mathrm{Tr}\{\boldsymbol{W}\}+\frac{1}{4M}\mathrm{Tr}\{\boldsymbol{T}\}\\&\text{s. t.}\quad \begin{bmatrix}\boldsymbol{W} & \boldsymbol{X}_0^{(\mathrm{nc})\mathrm{H}}\\ \boldsymbol{X}_0^{(\mathrm{nc})} & \boldsymbol{T}\end{bmatrix}\succeq\boldsymbol{0},\;\left\|\boldsymbol{X}^{(\mathrm{nc})}-\boldsymbol{X}_0^{(\mathrm{nc})}\right\|_{\mathrm{F}}^2\leq\eta^{(\mathrm{nc})}.\end{aligned}\tag{15}$$

The regularization parameter $\eta^{(\mathrm{nc})}$ is chosen according to the noise statistics, e.g., $\eta^{(\mathrm{nc})}=\mathrm{E}\{\|\boldsymbol{N}^{(\mathrm{nc})}\|_{\mathrm{F}}^2\}$. The spatial frequencies of interest along with the rotation phases and the signal powers are encoded in $\boldsymbol{T}$. Given the solution $\boldsymbol{T}$, the desired spatial frequencies can be retrieved by applying the multi-dimensional generalization of the Caratheodory theorem from [10], which states that any multi-level positive semi-definite Toeplitz matrix can be represented by a unique multi-dimensional Vandermonde decomposition with Kronecker structure. Consequently, for the NC case, we obtain the two-dimensional Vandermonde decomposition

$$\begin{aligned}\boldsymbol{T}&=\boldsymbol{A}^{(\mathrm{nc})}(\tilde{\boldsymbol{\mu}},\tilde{\boldsymbol{\varphi}})\boldsymbol{Z}\boldsymbol{A}^{(\mathrm{nc})\mathrm{H}}(\tilde{\boldsymbol{\mu}},\tilde{\boldsymbol{\varphi}})&(16)\\&=\sum_{k=1}^{K}c_k\boldsymbol{a}^{(\mathrm{nc})}(\tilde{\mu}_k,\tilde{\varphi}_k)\boldsymbol{a}^{(\mathrm{nc})\mathrm{H}}(\tilde{\mu}_k,\tilde{\varphi}_k),&(17)\end{aligned}$$

where $\boldsymbol{Z}=\mathrm{diag}\{c_1,\ldots,c_K\}$ contains the coefficients $c_k>0,\;k=1,\ldots,K$, on its diagonal,

$$\boldsymbol{a}^{(\mathrm{nc})}(\tilde{\mu}_k,\tilde{\varphi}_k)=\begin{bmatrix}\mathrm{e}^{\mathrm{j}\tilde{\varphi}_k}\\ \mathrm{e}^{-\mathrm{j}\tilde{\varphi}_k}\end{bmatrix}\otimes\boldsymbol{a}(\tilde{\mu}_k),\tag{18}$$

and $\mathrm{rank}\{\boldsymbol{T}\}=K\leq 2(M-1)$. The multi-dimensional Vandermonde decomposition in (17) can be obtained by estimating the spatial frequencies $\tilde{\mu}_k$ via subspace-based methods such as NC Standard/Unitary ESPRIT applied to the two-level Toeplitz matrix $\boldsymbol{T}$.

Remark 1: After recovery of the spatial frequencies $\tilde{\mu}_k$ from the two-level Toeplitz matrix $\boldsymbol{T}$, the reconstruction of the rotation phases $\tilde{\varphi}_k$ and the signal amplitudes c_k, for $k=1,\ldots,K$, can be performed as follows: Expand the two-level Toeplitz matrix $\boldsymbol{T}$ in (16) by using (6), the assumption that $\boldsymbol{\Delta}=\boldsymbol{I}_d$, and the fact that $\boldsymbol{Z}$ and $\boldsymbol{\Psi}(\tilde{\boldsymbol{\varphi}})$ are diagonal matrices as

$$\boldsymbol{T}=\begin{bmatrix}\boldsymbol{A}(\tilde{\boldsymbol{\mu}})\boldsymbol{Z}\boldsymbol{A}^{\mathrm{H}}(\tilde{\boldsymbol{\mu}}) & \boldsymbol{A}(\tilde{\boldsymbol{\mu}})\boldsymbol{Z}\boldsymbol{\Psi}^2(\tilde{\boldsymbol{\varphi}})\boldsymbol{A}^{\mathrm{H}}(\tilde{\boldsymbol{\mu}})\\ \boldsymbol{A}(\tilde{\boldsymbol{\mu}})\boldsymbol{Z}\boldsymbol{\Psi}^{-2}(\tilde{\boldsymbol{\varphi}})\boldsymbol{A}^{\mathrm{H}}(\tilde{\boldsymbol{\mu}}) & \boldsymbol{A}(\tilde{\boldsymbol{\mu}})\boldsymbol{Z}\boldsymbol{A}^{\mathrm{H}}(\tilde{\boldsymbol{\mu}})\end{bmatrix}.\tag{19}$$

Then, consider the (1,2)-Toeplitz block

$$\boldsymbol{T}_2=\boldsymbol{A}(\tilde{\boldsymbol{\mu}})\boldsymbol{Z}\boldsymbol{\Psi}^2(\tilde{\boldsymbol{\varphi}})\boldsymbol{A}^{\mathrm{H}}(\tilde{\boldsymbol{\mu}})\tag{20}$$

of (19) and define the vector $\boldsymbol{b}$ as the first column of $\boldsymbol{A}^{\mathrm{H}}(\tilde{\boldsymbol{\mu}})$, i.e.,

$$\boldsymbol{b}=\left[\mathrm{e}^{\mathrm{j}\frac{M-1}{2}\tilde{\mu}_1},\ldots,\mathrm{e}^{\mathrm{j}\frac{M-1}{2}\tilde{\mu}_K}\right]^{\mathrm{T}}.\tag{21}$$

Subsequently, the first column vector $\boldsymbol{t}$ of the Toeplitz block $\boldsymbol{T}_2$ in (20) can be expressed in the linear form

$$\boldsymbol{t}=\boldsymbol{A}(\tilde{\boldsymbol{\mu}})\boldsymbol{Z}\boldsymbol{\Psi}^2(\tilde{\boldsymbol{\varphi}})\boldsymbol{b}=\boldsymbol{A}(\tilde{\boldsymbol{\mu}})\boldsymbol{d},\tag{22}$$

where the vector

$$\begin{aligned}\boldsymbol{d}&=\boldsymbol{Z}\boldsymbol{\Psi}^2(\tilde{\boldsymbol{\varphi}})\boldsymbol{b}\\&=\left[c_1\mathrm{e}^{\mathrm{j}(2\tilde{\varphi}_1+\frac{M-1}{2}\tilde{\mu}_1)},\ldots,c_K\mathrm{e}^{\mathrm{j}(2\tilde{\varphi}_K+\frac{M-1}{2}\tilde{\mu}_K)}\right]^{\mathrm{T}}\end{aligned}\tag{23}$$

contains the unknown signal amplitudes c_k and the unknown rotation phases $\tilde{\varphi}_k$ in combination with the recovered spatial frequencies $\tilde{\mu}_k$, for $k=1\ldots,K$. By solving the linear system in (22) for $\boldsymbol{d}$, the signal amplitudes c_k and the rotation phases $\tilde{\varphi}_k$ can be extracted according to the relation in (23). Note that the rotation phases $\tilde{\varphi}_k$, $k=1,\ldots,K$, can only be uniquely recovered up to a multiple of π, since $\boldsymbol{S}=\boldsymbol{\Psi}(\boldsymbol{\varphi})\boldsymbol{S}_0=(-\boldsymbol{\Psi}(\boldsymbol{\varphi}))(-\boldsymbol{S}_0)$, according to the definition in Section II.

Remark 2: It was shown in [9] that the frequency separation condition for exact frequency recovery from the 1-D case in [6] also holds in the 2-D case and therefore applies here as well. However, as demonstrated in the simulation section, in the specific case of two uncorrelated NC sources with maximum phase separation, these sources entirely decouple such that the resolution limit does not apply in this case.

Remark 3: An important feature of the presented NC ANM approach is that it can resolve more sources than the number of physical sensors. This is due to the NC preprocessing, which virtually doubles the number of sensor elements. This property is shown via simulation results in Section IV.

B. Signal Subspace Processing

In the case $N>d$, solving the SDP problem in (15) may still require a substantial computational complexity. Following [17], this cost can be significantly decreased by operating on the signal subspace of $\boldsymbol{X}^{(\mathrm{nc})}$ instead of directly processing $\boldsymbol{X}^{(\mathrm{nc})}$. Thereby, the number of columns of the data is reduced from N to d.

Suppose the singular value decomposition of $\boldsymbol{X}^{(\mathrm{nc})}$ is given by $\boldsymbol{X}^{(\mathrm{nc})}=\boldsymbol{U}\boldsymbol{\Sigma}\boldsymbol{V}^{\mathrm{H}}$. Then, from the temporal covariance matrix

$$\boldsymbol{X}^{(\mathrm{nc})\mathrm{H}}\boldsymbol{X}^{(\mathrm{nc})}=\boldsymbol{X}^{\mathrm{H}}\boldsymbol{X}+\boldsymbol{X}^{\mathrm{T}}\boldsymbol{X}^{*}=2\,\mathrm{Re}\left\{\boldsymbol{X}^{\mathrm{H}}\boldsymbol{X}\right\}\in\mathbb{R}^{N\times N},$$

there must be a real-valued unitary basis $\boldsymbol{V}\in\mathbb{R}^{N\times N}$ for the row space of $\boldsymbol{X}^{(\mathrm{nc})}$. Decomposing $\boldsymbol{V}$ into $\boldsymbol{V}=[\boldsymbol{V}_{\mathrm{s}},\boldsymbol{V}_{\mathrm{n}}]$, where $\boldsymbol{V}_{\mathrm{s}}\in\mathbb{R}^{N\times d}$ contains the dominant right singular vectors of $\boldsymbol{V}$, we can reduce the dimensions of $\boldsymbol{X}_0^{(\mathrm{nc})}\in\mathbb{C}^{2M\times N}$ and $\boldsymbol{X}^{(\mathrm{nc})}\in\mathbb{C}^{2M\times N}$ to

$$\boldsymbol{X}_{\mathrm{sv}_0}^{(\mathrm{nc})}=\boldsymbol{X}_0^{(\mathrm{nc})}\boldsymbol{V}_{\mathrm{s}}\in\mathbb{C}^{2M\times d},\quad\boldsymbol{X}_{\mathrm{sv}}^{(\mathrm{nc})}=\boldsymbol{X}^{(\mathrm{nc})}\boldsymbol{V}_{\mathrm{s}}\in\mathbb{C}^{2M\times d}.\tag{24}$$

TABLE I
THE PROPOSED NC ANM ALGORITHM

1. NC preprocessing:

- Compute the augmented measurement matrix $\boldsymbol{X}^{(\mathrm{nc})} \in \mathbb{C}^{2M\times N}$ according to (2).

2. NC atomic norm minimization:

- Calculate $\boldsymbol{V}_{\mathrm{s}}$ from the SVD of $\boldsymbol{X}^{(\mathrm{nc})}$ required for the subspace processing in (24) if $N > d$.
- Solve the NC ANM SDP problem in (25) (if $N > d$) or that in (15) to obtain the two-level Toeplitz matrix $\boldsymbol{T}$.

3. Frequency estimation:

- Apply the NC Standard/Unitary ESPRIT algorithm to $\boldsymbol{T}$ to estimate the spatial frequencies $\mu_i,\ i = 1,\ldots,d$.

4. Signal amplitude and rotation phase estimation:

- Solve the linear system in (22).
- Recover the signal amplitudes c_i and rotation phases φ_i, $i = 1,\ldots,d$ according to (23).

Subsequently, the SDP problem in (15) can be reformulated as

$$\min_{\boldsymbol{W},\boldsymbol{T}} \quad \frac{1}{2}\mathrm{Tr}\{\boldsymbol{W}\} + \frac{1}{4M}\mathrm{Tr}\{\boldsymbol{T}\} \tag{25}$$
$$\text{s. t.} \quad \begin{bmatrix} \boldsymbol{W} & \boldsymbol{X}_{\mathrm{sv}_0}^{(\mathrm{nc})\mathrm{H}} \\ \boldsymbol{X}_{\mathrm{sv}_0}^{(\mathrm{nc})} & \boldsymbol{T} \end{bmatrix} \succeq \boldsymbol{0},\ \left\|\boldsymbol{X}_{\mathrm{sv}}^{(\mathrm{nc})} - \boldsymbol{X}_{\mathrm{sv}_0}^{(\mathrm{nc})}\right\|_{\mathrm{F}}^2 \le \eta_{\mathrm{sv}}^{(\mathrm{nc})},$$

whose solution can be obtained at a significantly lower computational complexity. Considering the selection of the regularization parameter $\eta_{\mathrm{sv}}^{(\mathrm{nc})}$, we follow the idea in [2], similar to the discussion in [17]. We choose $\eta_{\mathrm{sv}}^{(\mathrm{nc})}$ according to the noise statistics such that it provides an upper bound on the noise power with high probability γ, i.e.,

$$P\big(\|\boldsymbol{N}_{\mathrm{sv}}^{(\mathrm{nc})}\|_{\mathrm{F}}^2 \le \eta_{\mathrm{sv}}^{(\mathrm{nc})}\big) = \gamma. \tag{26}$$

In the case that the noise matrix $\boldsymbol{N}$, in $\boldsymbol{N}^{(\mathrm{nc})} = [\boldsymbol{N}^{\mathrm{T}}, (\boldsymbol{\Pi}_M\boldsymbol{N})^{\mathrm{H}}]^{\mathrm{T}}$, has independent and identically distributed (i.i.d.) Gaussian entries and for moderate to high SNR, $\|\boldsymbol{N}_{\mathrm{sv}}^{(\mathrm{nc})}\|_{\mathrm{F}}^2 = \|\boldsymbol{N}^{(\mathrm{nc})}\boldsymbol{V}\boldsymbol{K}\|_{\mathrm{F}}^2$ has approximately a χ^2-distribution with Md degrees of freedom upon its normalization by the noise variance $2\sigma_{\mathrm{n}}^2$. The reason that this holds only approximately is that the SVD of $\boldsymbol{X}^{(\mathrm{nc})}$ depends on the particular realization of the noise, and hence, the matrix $\boldsymbol{V}$ is a function of $\boldsymbol{N}^{(\mathrm{nc})}$.

The main steps of the proposed NC ANM algorithm are summarized in Table I.

IV. Simulation Results

In this section, we present simulation results that demonstrate the performance of the proposed NC ANM approach in comparison with existing algorithms. In particular, we compare the proposed NC ANM algorithm combined with NC Standard ESPRIT (NC ANM SE) to its non-NC counterpart (ANM SE) as well as the spatially smoothed versions of NC Standard ESPRIT (NC SE + SS) [18] and Standard ESPRIT (SE + SS) with least squares that are based on the sample covariance estimate. The algorithms are benchmarked by the deterministic Cramér-Rao bound (Det CRB) [19] and the deterministic NC CRB (Det NC CRB) [20].

In the first experiment, we assume a uniform linear array (ULA) with $M = 12$ isotropic sensors. The phase reference of the array is located at the array centroid. The received signals are orthogonal with unit power and their transmitted symbols are drawn from a real-valued Gaussian distribution. Moreover, we assume zero-mean circularly symmetric white sensor noise. The number of subarrays L for spatial smoothing is $L = 4$. The regularization parameters are chosen according to (26) for $\gamma = 0.99$. The curves are obtained by averaging over 1000 Monte Carlo trials.

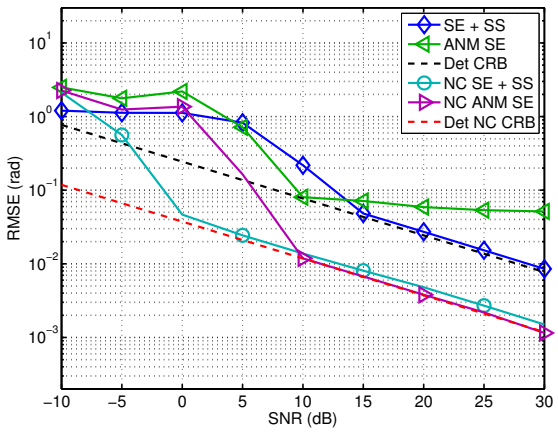

Fig. 1. RMSE versus the SNR for $d = 2$ at $\mu_1 = 1$ and $\mu_1 = 1.1$ with $M = 12$, $N = 5$, $L = 4$, and $\varphi_1 = 0$ and $\varphi_2 = \pi/2$.

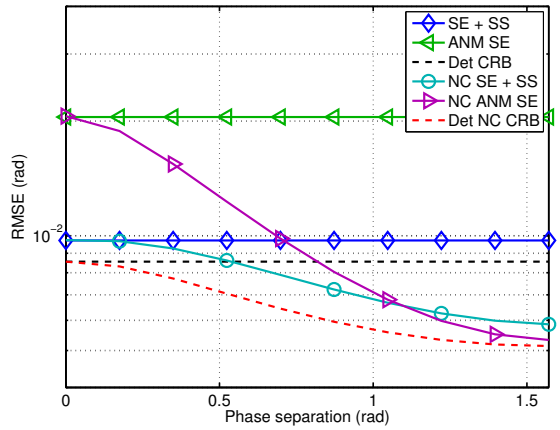

Fig. 2. RMSE versus the phase separation $\Delta\varphi = |\varphi_2 - \varphi_1|$ for $d = 2$ at $\mu_1 = 0.5$ and $\mu_1 = 0.9$ with $M = 12$, $N = 5$, $L = 4$, and SNR = 20 dB.

Fig. 1 illustrates the RMSE as a function of the SNR for $d = 2$ sources from the directions $\mu_1 = 1$ and $\mu_2 = 1.1$ with the rotation phases $\varphi_1 = 0$ and $\varphi_2 = \pi/2$. We assume $N = 5$ snapshots. It can be seen that while ANM SE produces a bias due to the violated resolution limit as $\Delta\mu = |\mu_2 - \mu_1| = 0.1$, the proposed NC ANM SE algorithm does not suffer from the resolution limit due to the entire decoupling of the two sources at $\Delta\varphi = |\varphi_2 - \varphi_1| = \pi/2$. Moreover, NC ANM SE has a superior performance over the NC SE + SS algorithm for higher SNRs and achieves the Det NC CRB.

In Fig. 2, we analyze the RMSE as a function of the phase separation $\Delta\varphi = |\varphi_2 - \varphi_1|$. We again consider $d = 2$ sources located at $\mu_1 = 0.5$ and $\mu_2 = 0.9$. We have $N = 5$ snapshots and the SNR is set to $\mathrm{SNR} = 20$ dB. It is apparent from Fig. 2 that the RMSE of the NC algorithms reduces for an increasing phase separation while the RMSE of the non-NC versions remains constant. The reason for this behavior in the NC case is again the spatial decorrelation of two

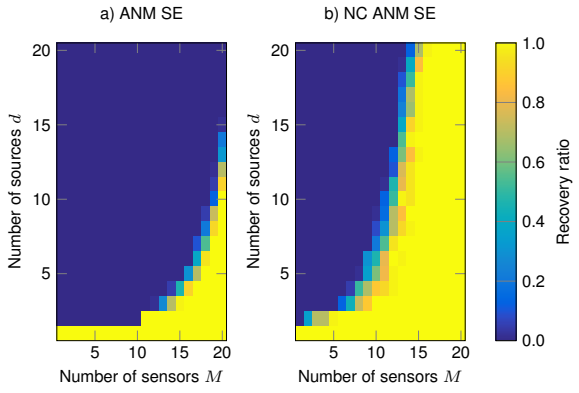

Fig. 3. Frequency recovery ratio of a) ANM with Standard ESPRIT and b) NC ANM with NC Standard ESPRIT.

closely-spaced sources due to the phase discrimination. It is also clear that NC ANM SE outperforms NC SE + SS close to $\Delta\varphi = \pi/2$.

In the second experiment, we compare the recovery performance of the proposed NC ANM SE algorithm to its non-NC counterpart ANM SE in the noise-free case, i.e., $\sigma_{\mathrm{n}}^2 = 0$. We assume $N = 10$ snapshots and vary the number of sensors M and the number of source signals d. The spatial frequency of the i-th source is given as $\mu_i = i \cdot \pi/10$ while its rotation phase is given as $\varphi_i = i \cdot \pi/2$, for $i = 1, \ldots, d$. Fig. 3 shows the ratio of successful frequency recovery for 100 Monte Carlo trials with real-valued uncorrelated Gaussian source signals with the covariance matrix $\mathbb{E}\{\boldsymbol{S}_0\boldsymbol{S}_0^{\mathrm{T}}\} = N\boldsymbol{I}_d$. From Fig. 3a), it can be seen that ANM SE cannot recover the frequencies in most of the scenarios, which is due to the close frequency spacing of $\Delta\mu = 0.314$. On the other hand, Fig. 3b) shows a significantly improved recovery ratio for the proposed NC ANM SE algorithm, which is caused by the optimal rotation phase difference of $\Delta\varphi = \pi/2$ between any two adjacent source signals. Furthermore, the plot demonstrates well that NC ANM SE admits the identifiability of more signals d than sensors M, e.g., $d = 20$ source signals can be resolved with $M = 16$ sensors.

V. Conclusion

In this paper, we have introduced an extension of the MMV-based ANM framework, termed NC ANM algorithm, which takes additional signal structure into account by exploiting the statistical properties of NC signals. Due to the NC preprocessing step, the NC ANM problem becomes a 2-D problem, which provides a two-level Hermitian Toeplitz structured solution matrix. The desired spatial frequencies are then extracted from the Toeplitz matrix via NC Standard/Unitary ESPRIT in closed-form, which results in a reduced estimation error and an increased source identifiability compared to the conventional ANM algorithm. Moreover, we have shown in simulations that due to the decoupling effect of two NC sources with maximum phase separation, the NC ANM approach does not suffer from the resolution limit.

References

[1] H. Krim and M. Viberg, "Two decades of array signal processing research: the parametric approach," *IEEE Signal Processing Magazine*, vol. 13, no. 4, pp. 67-94, July 1996.

[2] D. Malioutov, M. Cetin, and A. S. Willsky, "A sparse signal reconstruction perspective for source localization with sensor arrays," *IEEE Transactions on Signal Processing*, vol. 53, no. 8, pp. 3010-3022, Aug. 2005.

[3] M. M. Hyder and K. Mahata, "Direction-of-arrival estimation using a mixed $\ell_{2,0}$ norm approximation," *IEEE Transactions on Signal Processing*, vol. 58, no. 9, pp. 4646-4655, Sep. 2010.

[4] D. Donoho, "Superresolution via sparsity constraints," *SIAM Journal on Mathematical Analysis*, vol. 23, pp. 1309-1331, Sep. 1992.

[5] E. Candès, "Compressive sampling," in *Proc. of the International Congress of Mathematicians: Madrid*, August 22-30, 2006: invited lectures, 2006, pp. 1433-1452.

[6] E. J. Candés and C. Fernandez-Granda, "Towards a mathematical theory of super-resolution," *Communications on Pure and Applied Mathematics*, vol. 67, no. 6, pp. 906-956, 2014.

[7] G. Tang, B. N. Bhaskar, P. Shah, and B. Recht, "Compressed sensing off the grid," *IEEE Transactions on Information Theory*, vol. 59, no. 11, pp. 7465-7490, Nov. 2013.

[8] Z. Yang and L. Xie, "Exact joint sparse frequency recovery via optimization methods," *IEEE Transactions on Signal Processing*, vol. 64, no. 19, pp. 5145-5157, Oct 1, 2016.

[9] Y. Chi and Y. Chen, "Compressive two-dimensional harmonic retrieval via atomic norm minimization," *IEEE Transactions on Signal Processing*, vol. 63, no. 4, pp. 1030-1042, Feb. 2015.

[10] Z. Yang, L. Xie, and P. Stoica, "Vandermonde decomposition of multilevel Toeplitz matrices with application to multidimensional super-resolution," *IEEE Transactions on Information Theory*, vol. 62. no. 6, pp. 3685-3701, June 2016.

[11] P. J. Schreier and L. L. Scharf, *Statistical Signal Processing of Complex-Valued Data: The Theory of Improper and Noncircular Signals*, Cambridge, U.K.: Cambridge Univ. Press, 2010.

[12] H. Abeida and J. P. Delmas, "MUSIC-like estimation of direction of arrival for noncircular sources," *IEEE Transactions on Signal Processing*, vol. 54, no. 7, pp. 2678-2690, July 2006.

[13] A. Zoubir, P. Chargé, and Y. Wang, "Non circular sources localization with ESPRIT," in *Proc. European Conference on Wireless Technology (ECWT 2003)*, Munich, Germany, Oct. 2003.

[14] M. Haardt and F. Roemer, "Enhancements of Unitary ESPRIT for non-circular sources," in *Proc. IEEE Int. Conf. on Acoust., Speech, and Sig. Proc. (ICASSP)*, Montreal, Canada, May 2004.

[15] J. Steinwandt, F. Roemer, M. Haardt, and G. Del Galdo, "R-dimensional ESPRIT-type algorithms for strictly second-order non-circular sources and their performance analysis," *IEEE Transactions on Signal Processing*, vol. 62, no. 18, pp. 4824-4838, Sept. 2014.

[16] J. Steinwandt, F. Roemer, and M. Haardt, "Sparsity-based direction-of-arrival estimation for strictly non-circular sources," in *Proc. IEEE Int. Conf. on Acoust., Speech, and Sig. Proc. (ICASSP)*, Shanghai, China, March 2016.

[17] J. Steinwandt, C. Steffens, M. Pesavento, and M. Haardt, "Sparsity-aware direction finding for strictly non-circular sources based on rank minimization," in *Proc. IEEE Sensor Array and Multichannel Signal Processing Workshop (SAM)*, Rio de Janeiro, Brazil, July 2016.

[18] J. Steinwandt, F. Roemer, M. Haardt, and G. Del Galdo, "Performance analysis of multi-dimensional ESPRIT-type algorithms for arbitrary and strictly non-circular sources with spatial smoothing," arXiv:1610.02253, Oct. 2016.

[19] P. Stoica and A. Nehorai, "MUSIC, maximum likelihood, and Cramér-Rao bound," *IEEE Transactions on Acoustics, Speech and Signal Processing*, vol. 37, no. 5, pp. 720-741, May 1989.

[20] J. Steinwandt, F. Roemer, M. Haardt, and G. Del Galdo, "Deterministic Cramér-Rao bound for strictly non-circular sources and analytical analysis of the achievable gains," *IEEE Transactions on Signal Processing*, vol. 64, no. 17, pp. 4417-4431, Sept. 2016.